

Magnetic structure of the Er^{3+} moments in the charge-density-wave compound $\text{Er}_5\text{Ir}_4\text{Si}_{10}$

F. Galli,¹ R. Feyherherm,² R. W. A. Hendrikx,¹ S. Ramakrishnan,^{1,3} G. J. Nieuwenhuys,¹ and J. A. Mydosh¹

¹Kamerlingh Onnes Laboratory, Leiden University, 2300 RA Leiden, The Netherlands

²Hahn-Meitner-Institut, Glienicker Straße 100, D-14109 Berlin, Germany

³Tata Institute of Fundamental Research, Homi Bhabha Road, Mumbai 400 005, India

(Received 16 June 2000)

We report the magnetic structure of the local moment magnetism in high-quality single crystals of the intermetallic compound $\text{Er}_5\text{Ir}_4\text{Si}_{10}$, which shows two charge-density-wave (CDW) transitions ($T_{\text{CDW}}^{(1)}=155$ K and $T_{\text{CDW}}^{(2)}=55$ K). Bulk measurements demonstrate that the system has an effective Curie-Weiss magnetic moment of $9.7\mu_B$ and undergoes long-range antiferromagnetic (AFM) ordering at 2.8 K. The neutron-diffraction data establish the AFM structure of the Er^{3+} with unequal moments at different Er sites aligned along the c axis where also the CDW transitions occur.

Study of ternary rare-earth (R) intermetallic compounds of the type $R_5M_4\text{Si}_{10}$ (space group $P4/mbm$, M = transition metal)¹ is currently of interest due to their exotic magnetic orderings, crystal electric-field (CEF) effects, and collective phenomena, like superconductivity and charge-density waves (CDW's).²⁻⁶ In these systems the local-moment magnetism is mainly due to the Ruderman-Kittel-Kasuya-Yosida (RKKY) exchange, which is a long-range interaction between the localized $4f$ electrons, mediated by the itinerant conduction electrons. At the same time, possible existence of one-dimensional (1D) chains in this structure causes the nesting of the Fermi surfaces, which could lead to the occurrence of CDW at higher temperatures. This allows the unique possibility of studying the interplay between CDW and local-moment magnetism in this class of compounds.

Rare-earth iridium silicides, $R_5\text{Ir}_4\text{Si}_{10}$, are particularly suited for this purpose: The ones with magnetic rare-earth ions order magnetically at low temperatures and in some cases (heavy rare earths) also display anomalies in the resistivity at higher temperatures.^{2,3} These anomalies were tentatively attributed to either CDW or spin-density wave (SDW). The true nature of these transitions was not ascertained since measurements were performed on polycrystals without any high-resolution diffraction studies. Recently, we have established, via single-crystal x-ray diffraction,⁶ that $\text{Er}_5\text{Ir}_4\text{Si}_{10}$ shows a transition to an atypical incommensurate CDW (155 K), which locks in commensurately at 55 K. The CDW's take place along the c axis, with a q vector $(0,0,1/4 \pm \delta)$ below 155 K, and $(0,0,1/4)$ below 55 K. The first transition appears simultaneously with a commensurate structural transformation [$q=(0,0,1/2)$]. The system crystallizes in the tetragonal $\text{Sc}_5\text{Co}_4\text{Si}_{10}$ structure (space group $P4/mbm$) where Sc atoms occupy three different sites. The low dimensionality required for typical CDW behavior in $\text{Er}_5\text{Ir}_4\text{Si}_{10}$ can be visualized if one considers that the CDW occurs along the chains of Er1 atoms (along the c axis), embedded in a network of closely bonded Er2-Er3 atoms (see Fig. 1 in Refs. 5 and 6).

In this paper we present the magnetic order and structure of the Er^{3+} moments in the CDW modulated lattice of

$\text{Er}_5\text{Ir}_4\text{Si}_{10}$ via bulk measurements and neutron diffraction. Two single-crystal samples of $\text{Er}_5\text{Ir}_4\text{Si}_{10}$ have been synthesized in a tri-arc crystal puller using the Czochralski technique⁷ (pulling rate 5 mm/hour; seed rotation 15 rpm). The purity of the elements (melted in a stoichiometric ratio) was Er:4N, Ir:4N, and Si:5N. The quality of the crystals was analyzed using electron-probe microanalysis (EPMA) which proved them to be single phase (secondary phases <1%) and to have the correct 5:4:10 stoichiometry (within 2% resolution). The single-crystalline nature of the samples was verified using a Laue diffraction technique.

The magnetic susceptibility (χ), the electrical resistivity (ρ), and the specific heat (C_p) were measured, from 1.8 to 300 K, on oriented small bars of the single crystals. For these measurements a Quantum Design magnetometer (MPMS, Magnetic Property Measurement System) and Physical Property Measurement System (PPMS) were used. Powder and single-crystal neutron diffraction were performed at the neutron facility (BENS) of the Hahn-Meitner Institut, Berlin.

Previous measurements of electrical resistivity and magnetic susceptibility on polycrystalline samples^{2,3} showed an-

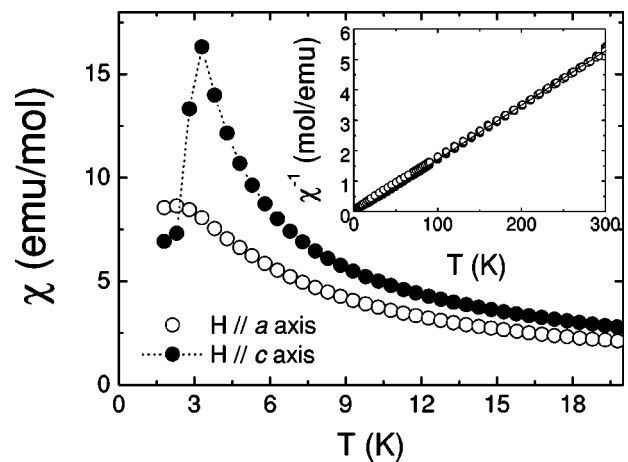


FIG. 1. Temperature dependence of the dc susceptibility for $\text{Er}_5\text{Ir}_4\text{Si}_{10}$, below 20 K. The sharp cusp (broader along the a axis) indicates the antiferromagnetic ordering at $T_N=2.8$ K. The inset displays the inverse of the dc susceptibility vs temperature, and the solid line is a Curie-Weiss fit to the data.

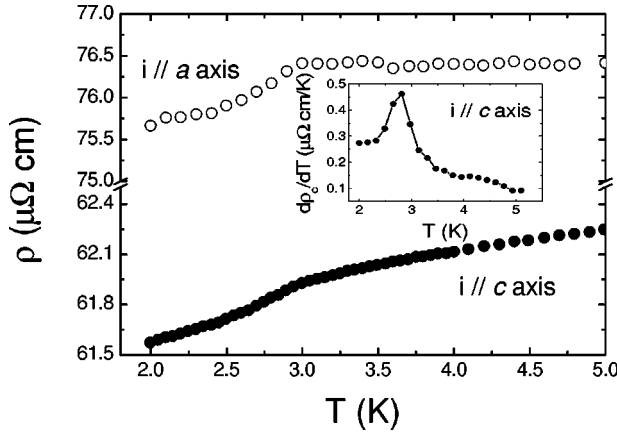


FIG. 2. Low-temperature resistivity for current along a and c axes. The change of slope in ρ indicates the onset of the antiferromagnetic ordering. The inset shows the temperature derivative of the resistivity ($d\rho/dT$).

tiferromagnetic ordering around 3 K. Our single-crystal data of dc susceptibility are presented in Fig. 1. The temperature dependence of the inverse of χ_{dc} (see inset of Fig. 1) exhibits a Curie-Weiss behavior from 300 K down to about 20 K, where the data deviate slightly from linearity. This can be ascribed to the CEF effects. In the Curie-Weiss regime no anisotropy is observed, while below 20 K the χ_{dc} with field along the a axis is smaller than the one with field along the c axis. The effective moment is found to be $9.7\mu_B$, in agreement with the expected value for the Er^{3+} free ion, and $\theta_p = -3.0$ K. For $T < 2.8$ K the system orders antiferromagnetically, whereby the magnetic susceptibility shows a sharp cusp along the c axis and a broader anomaly along the a axis, as depicted in Fig. 1.

Heat-capacity data⁸ show a λ -type anomaly (with $S = 0.6 R \ln 2$ per mole Er, at T_N) suggesting a second-order transition at 2.8 K and establishing the bulk antiferromagnetic ordering in $\text{Er}_5\text{Ir}_4\text{Si}_{10}$. Figure 2 displays the low-temperature electrical resistivity along a and c axes. The change in slope of ρ (peak in $d\rho/dT$ in the inset of Fig. 2) indicates the antiferromagnetic transition. No hysteresis effect was observed either in χ or ρ above and below the antiferromagnetic transition.

Powder and single-crystal neutron diffraction have been carried out on the BENS C diffractometers E2 and E6. Both diffractometers are equipped with multichannel detectors, covering a range of scattering angles of 80° and 20° , respectively. To allow for the detection of low indexed Bragg reflections, relatively long wavelengths of 2.406 and 2.448 Å, respectively, were used. To account for the strong absorption of neutrons by Er and Ir, resulting in a bulk absorption length $\mu^{-1} = 1$ mm, the sample diameters were kept small (2–3 mm). The powder sample was cooled in a flow cryostat, while the single-crystal diffraction experiment was performed using a $^3\text{He}/^4\text{He}$ dilution refrigerator. The analysis of the diffraction data was carried out using GSAS (General Structure Analysis System).⁹

From powder diffractograms collected at 1.7 and 3.5 K (not shown) a number of Bragg reflections of magnetic origin, appearing on cooling below T_N , were identified. Almost all these peaks could be indexed as $(h/2, k/2, 0)$, $h, k = \text{odd}$.

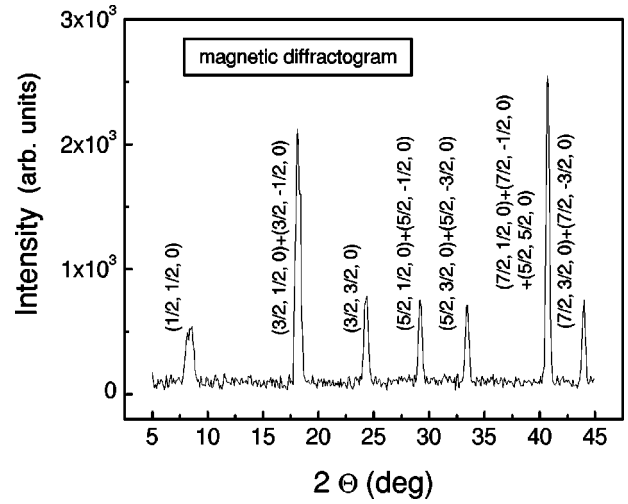


FIG. 3. Difference between the diffractogram at 2 K (antiferromagnetic state) and the one at 4 K (paramagnetic state). Only Bragg reflections of magnetic origin remain.

This corresponds to the propagation vector $\mathbf{k} = (1/2, 1/2, 0)$. In order to improve the statistical data quality we subsequently performed single-crystal diffraction measurements. The cylindrical sample was mounted with the c axis, coinciding with the cylinder axis, perpendicular to the scattering plane. Therefore in the experiment a full quadrant of the $(hk0)$ scattering plane could be scanned by slowly rotating the sample around the vertical ω axis by about 100° and collecting the scattered neutrons in the multichannel detectors. This procedure ensures that no Bragg reflections in the scattering plane can be accidentally overlooked.

The resulting magnetic diffractogram after integration over ω is displayed in Fig. 3. At $T = 2$ K we observe only reflections of type $(h/2, k/2, 0)$, $h, k = \text{odd}$, which is consistent with the above propagation vector derived from the powder data. This implies a doubling of the unit cell along the two directions in the basal plane. The corresponding unit cell of size $2a \times 2a \times c$ contains 40 Er ions. Obviously, one has to make use of symmetry arguments to reduce the number of free parameters for building a model of the magnetic structure.

We arrive at the simplest model consistent with the data as follows:

(i) The propagation vector $\mathbf{k} = (1/2, 1/2, 0)$ implies that the two basal plane diagonals of the original tetragonal cell become inequivalent and consequently the magnetic symmetry is orthorhombic.

(ii) The magnetic structure can be represented in a cell which is rotated by 45° with respect to the original cell with cell parameters $a' = b' = a\sqrt{2}$. This is the smallest magnetic unit cell consistent with the mentioned propagation vector and contains only 20 Er ions. Most of the symmetry elements of the original cell are conserved in the orthorhombic space group $Cmmm$. In this cell the Er1 ions are located at $(1/4, 1/4, 0)$ equivalent positions. The positions Er2 and Er3 split up into two subsets, Er2a/Er3a $(0, y, 1/2)$ and Er2b/Er3b $(x, 0, 1/2)$.

(iii) All moments located in common planes perpendicular to \mathbf{k} are assumed to carry equal magnetic moments. This results in ferromagnetic sheets stacked along \mathbf{k} .

TABLE I. Observed magnetic integrated intensities [$I(2\text{ K})-I(4\text{ K})$] and calculated intensities (I_{cal}) from the fit of the magnetic structure with the model described in the text. All the intensities are normalized to the $(3/2, 1/2, 0) + (3/2, -1/2, 0)$ calculated intensity. The calculated reliability factor for this fit is 0.5%.

| hkl | 2θ (deg) | $I(2\text{ K})-I(4\text{ K})$ | I_{cal} |
|----------------------------------|-----------------|-------------------------------|-----------|
| $(1/2, 1/2, 0)$ | 8.41 | 31.83 | 32.50 |
| $(3/2, 1/2, 0) + (3/2, -1/2, 0)$ | 18.18 | 99.67 | 100 |
| $(3/2, 3/2, 0)$ | 24.33 | 30.06 | 30.10 |
| $(5/2, 1/2, 0) + (5/2, -1/2, 0)$ | 29.22 | 24.0 | 24.0 |
| $(5/2, 3/2, 0) + (5/2, -3/2, 0)$ | 33.45 | 22.53 | 22.65 |
| $(5/2, 5/2, 0)$ | 40.75 | 29.08 | 29.19 |
| $(7/2, 1/2, 0) + (7/2, -1/2, 0)$ | 40.75 | 33.04 | 32.93 |
| $(7/2, 3/2, 0) + (7/2, -3/2, 0)$ | 43.98 | 20.59 | 20.61 |

(iv) The presence of the reflections of type $(h/2, h/2, 0)$ shows that the magnetic moments are not parallel to \mathbf{k} , i.e., not perpendicular to the sheets.

(v) The small intensity of reflections of type $(h/2, k/2, 1)$ observed in the powder data with small h, k indicates that the moments are oriented parallel to c . This is consistent with the pronounced reduction of χ_{dc} below T_N (see Fig. 1).

All these points lead to a representation of the magnetic structure in the magnetic space group $Pm'mm$. In the resulting magnetic structure model there are only three free parameters, namely the absolute values of the magnetic moments on the Er1, Er2b, and Er3b ions. The magnetic moments at the Er2a and Er3a ions, which are located on two perpendicular mirror planes, are forced to be zero for symmetry reasons, namely conflicting time reversal operations for the mirror planes.

Table I lists the measured intensities and the ones resulting from the best fit of this magnetic structure model to the data. An absorption correction has been included. The absolute values of the ordered moments are determined by comparison of the intensities of the magnetic with the nuclear Bragg reflections. The fit results in different absolute values for the magnetic moments on the three types of Er ions, namely $9.0(2)\mu_B$ for Er1, $1.4(2)\mu_B$ for Er2b, and $2.0(2)\mu_B$ for Er3b. The resulting magnetic structure is shown in Fig. 4. The small value of the entropy S at T_N is most likely due to the fact that the Er2b and Er3b have reduced moments. From Table I, one can see that the model describes the data very well, which gives us confidence that the above simplifications are valid.

In the single-crystal diffraction experiment below 1.4 K some weak additional reflections were observed, indicating a second magnetic transition for which indications were found already in our measurements of the transport properties at very low T .¹⁰ The new reflections are of type $(h/4, k/4, 0)$, $h, k = \text{odd}$, indicating a superstructure with another doubling of the magnetic unit cell. The new magnetic unit cell has the dimension $35.5 \times 35.5 \times 4.2 \text{ \AA}$. The intensities of these new reflections is found to be only a few percent of the original magnetic reflections of type $(h/2, k/2, 0)$. We also observe an increase of the intensity of the $(h/2, h/2, 0)$ peaks. Due to the weakness of the extra reflections the quantitative analysis is difficult. We presume, however, that the superstructure is associated with an increase of the ordered moments at the Er2 and Er3 sites and a small modulation of the magnitude of the Er magnetic moments.

Figure 5 displays the temperature dependence of the square root of the integrated intensity of the $(3/2, 3/2, 0)$ line, normalized to its value at $T=1.89\text{ K}$. This reflects the temperature-dependent behavior of the magnetically ordered moments and supports the hypothesis of a continuous phase transition at 2.8 K.

In these systems the magnetic ordering is determined by the localized $4f$ electrons of the magnetic rare-earth element, which, in first approximation, can be thought as free ions with a given valency. Moreover, charge-density distributions surrounding the f electrons and affecting the orbital part of their wave function, are responsible for the CEF whose symmetry is determined by the lattice structure. The RKKY interaction generally supports long-range interaction between local moments, via conduction electrons. Polycrystalline sample studies^{2,3} disagree with the de Gennes scaling,¹¹ suggesting that the main interaction leading to the magnetism in these systems is not purely RKKY and it is modified by CEF which generally can enhance or even decrease the T_N .¹² However, the low value of T_N in $\text{Er}_5\text{Ir}_4\text{Si}_{10}$ could also be caused by the decrease in the conduction electrons density of states due to the gap formation arising from CDW transitions. The fact that the Er^{3+} moments are aligned along the c axis is in agreement with the observation that such an align-

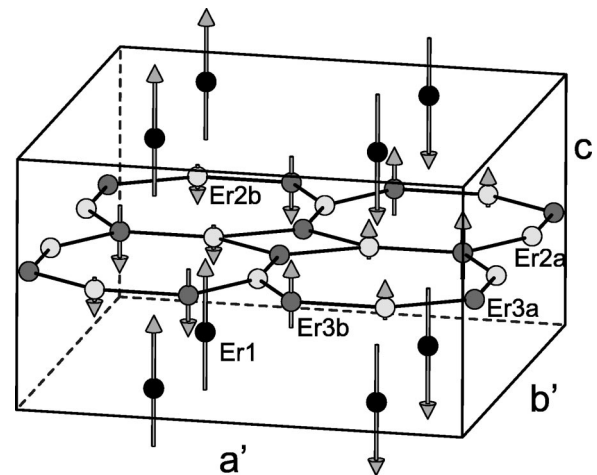


FIG. 4. Magnetic unit cell. Only the Er atoms are shown, with the new five inequivalent positions. The ordered moments are different from site to site, and for symmetry reasons are zero on the Er2a and Er3a sites (see text). For clarity, the c axis is expanded by a factor of 2.

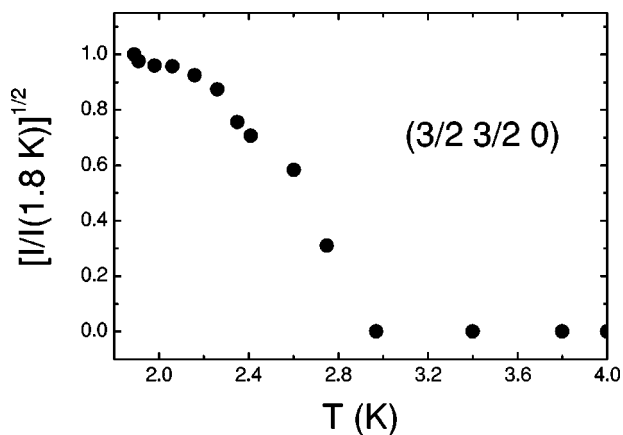


FIG. 5. Temperature dependence of the square root of the integrated intensity of the $(3/2, 3/2, 0)$ line, normalized to its value at $T=1.89$ K.

ment is not found in the isostructural single-crystal $\text{Nd}_5\text{Rh}_4\text{Sn}_{10}$,^{13,14} which does not exhibit any CDW transition. Our striking observation is that the periodic lattice distortion caused by the CDW occurs along the c axis, most

probably along the Er1 chain, where the localized magnetic moments have their saturation value.

In summary, our investigations of the low-temperature bulk properties (χ_{dc} , C_p and ρ) and of the magnetic structure (via neutron scattering) on high quality single crystals of $\text{Er}_5\text{Ir}_4\text{Si}_{10}$, clearly demonstrate that the system undergoes to a continuous phase transition to a local-moment antiferromagnetic structure below 2.8 K. The magnetic structure is such that CDW and local-moment magnetism may coexist along the c axis. We believe that $\text{Er}_5\text{Ir}_4\text{Si}_{10}$ is the first system where this behavior occurs and detail understanding of the interplay between these two collective phenomena requires the determination of CEF levels and uniaxial pressure dependence of both CDW and antiferromagnetism.

The authors gratefully acknowledge R. Schneider, M. Hofmann, and P. Smeibidl for their assistance in the neutron-scattering experiments. The crystals were grown at FOM-ALMOS under the supervision of A. A. Menovsky. We would like to thank T. Taniguchi for his help in the magnetic measurements. Part of this research was supported by the Dutch Foundation FOM and the European Commission under the TMR-LSF program.

¹H.F. Braun, *J. Less-Common Met.* **100**, 105 (1984); H.F. Braun, K. Yvon, and R. Braun, *Acta Crystallogr., Sect. B: Struct. Crystallogr. Cryst. Chem.* **36**, 2397 (1980).

²H.D. Yang, P. Klavins, and R.N. Shelton, *Phys. Rev. B* **43**, 7688 (1991).

³K. Ghosh, S. Ramakrishnan, and Girish Chandra, *Phys. Rev. B* **48**, 4152 (1993).

⁴N.G. Patil and S. Ramakrishnan, *Phys. Rev. B* **56**, 3360 (1997); **59**, 9581 (1999).

⁵B. Becker, N.G. Patil, S. Ramakrishnan, A.A. Menovsky, G.J. Nieuwenhuys, J.A. Mydosh, M. Kohgi, and K. Iwasa, *Phys. Rev. B* **59**, 7266 (1999).

⁶F. Galli, S. Ramakrishnan, T. Taniguchi, G.J. Nieuwenhuys, J.A. Mydosh, S. Geupel, J. Ludecke, and S. van Smaalen, *Phys. Rev. Lett.* **85**, 158 (2000).

⁷A.A. Menovsky and J.J.M. Franse, *J. Cryst. Growth* **65**, 286

(1983).

⁸F. Galli, T. Taniguchi, A.A. Menovsky, G.J. Nieuwenhuys, J.A. Mydosh, and S. Ramakrishnan, *Physica B* **281&282**, 171 (2000).

⁹A.C. Larson and R.B. van Dreele, Los Alamos National Laboratory Report No. LA-UCR-86-748, 1986.

¹⁰F. Galli, R. Feyerherm, S. Ramakrishnan, G.J. Nieuwenhuys, J.A. Mydosh (unpublished).

¹¹P.G. de Gennes, *J. Phys. Radium* **23**, 510 (1962).

¹²D.R. Noakes and G.K. Shenoy, *Phys. Lett.* **91A**, 35 (1982).

¹³N.G. Patil, S. Ramakrishnan, B. Becker, A.A. Menovsky, G.J. Nieuwenhuys, and J.A. Mydosh, *J. Appl. Phys.* **85**, 4845 (1999).

¹⁴Note that Nd^{3+} and Er^{3+} have a Stevens α factor with opposite sign. See, for example, M.T. Hutchings, *Solid State Phys.* **16**, 227 (1964).